Discovery of Retinoic Acid-Related Orphan Receptor γt Inverse Agonists via Docking and Negative Image-Based Screening

Sanna Rauhamäki,[†] Pekka A. Postila,[†] Sakari Lätti,[†,‡] Sanna Niinivehmas,[†,‡] Elina Multamäki,[†] Klaus R. Liedl,[§] and Olli T. Pentikäinen*[,†,‡,§]

[†]Department of Biological and Environmental Science & Nanoscience Center, University of Jyväskylä, P.O. Box 35, Jyväskylä FI-40014 University of Jyvaskyla, Finland

[‡]Institute of Biomedicine, Integrative Physiology and Pharmacology, Kiinamyllynkatu 10 C6, University of Turku, FI-20520 Turku, Finland

[§]Institute of General, Inorganic and Theoretical Chemistry, Centre for Chemistry and Biomedicine, University of Innsbruck, Innrain 82, A-6020 Innsbruck, Austria

S Supporting Information

CAVITY LOCATION • NEGATIVE IMAGE-BASED SCREENING • PHARMACOPHORE FILTERING
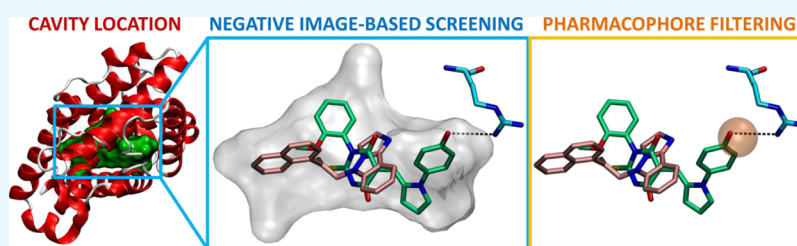
ABSTRACT: Retinoic acid-related orphan receptor γt (RORγt) has a vital role in the differentiation of T-helper 17 (TH17) cells. Potent and specific RORγt inverse agonists are sought for treating TH17-related diseases such as psoriasis, rheumatoid arthritis, and type 1 diabetes. Here, the aim was to discover novel RORγt ligands using both standard molecular docking and negative image-based screening. Interestingly, both of these in silico techniques put forward mostly the same compounds for experimental testing. In total, 11 of the 34 molecules purchased for testing were verified as RORγt inverse agonists, thus making the effective hit rate 32%. The pIC_{50} values for the compounds varied from 4.9 (11 μM) to 6.2 (590 nM). Importantly, the fact that the verified hits represent four different cores highlights the structural diversity of the RORγt inverse agonism and the ability of the applied screening methodologies to facilitate much-desired scaffold hopping for drug design.

INTRODUCTION

Retinoic acid receptor-related orphan receptor γt (RORγt; Figure 1) is a nuclear receptor expressed mainly in the thymus.[1] It is essential for the differentiation of proinflammatory CD4 + T-helper 17 (Th17) cells producing interleukin 17 (IL-17).[2] Normally, IL-17 expression is increased in response to pathogenic bacteria and fungi on mucous membranes, but its elevated production is also connected to inflammatory and autoimmune conditions such as multiple sclerosis, rheumatoid arthritis, and psoriasis.[3] Accordingly, RORγt is an attractive drug target for autoimmune diseases.[4,5] RORγt is isoform 2 of the RORC gene (UniProt: P51449-2), and it is almost identical to isoform 1 RORγ (UniProt: P51449-1) that has a longer N-terminus. Isoform 1 drives androgen receptor expression, and thus, it is also a target for castration-resistant prostate cancer.[6] Because of the similarity between the isoforms, the RORγt abbreviation refers to both isoforms from here on.

Thus far, a wide variety of RORγt inverse agonists have emerged.[7−19] Moreover, Vitae Pharma's VTP-43742 (acquired by Allergan plc) has reached phase II trials for the treatment of psoriasis. Importantly, there are 70 X-ray crystal structures of RORγt in both ligand-free and ligand-bound states (3QQ in

Figure 1A−C), providing atomistic insight. In the inverse agonist structures (e.g. PDB: 3L0L; 5APH; 4QM0),[20−22] the side chains of His479 and Tyr502 are hydrogen bonding (Figure 1C)—an interaction missing from bound full agonist RORγt structures (e.g. PDB: 5M96).[23]

The ligand-binding cavity of RORγt is highly lipophilic as indicated by its neutral negative image (Figure 1D). The lipophilicity is projected on its known ligands (Figure 1E). In fact, a high log P value seems to be needed to elicit activity (Figure 1E). Although this level of ligand neutrality is typical for nuclear receptors, the opposite is true for targets such as ionotropic glutamate receptors with extracellular binding sites.[24−26] Despite the cavity's lipophilicity, it contains some polar residues. For example, Arg367 at the sulfate pocket donates a hydrogen bond (H-Bond) to several potent RORγt ligands (Figure 1C; PDB: 4WLB).

In the structure-based drug design, the target protein three-dimensional (3D) structure is used in developing novel drug
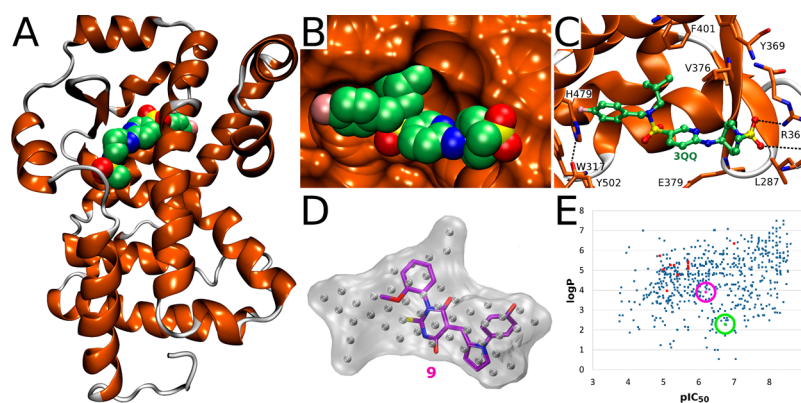
Figure 1. Binding site of RORγt. (A) 3D structure (cartoon; PDB: 4WLB) is shown with a bound partial inverse agonist 3QQ N-(4-fluorobenzyl)-N-(2-methylpropyl)-6-{[1-(methylsulfonyl)piperidin-4-yl]amino}pyridine-3-sulfonamide; green CPK backbone). (B) Cross section of the site demonstrates the complementarity of the ligand and its receptor (surface). (C) Key residues such as Arg367, that H-bond with the sulfonamide of 3QQ, are shown as sticks. (D) Negative image of the cavity (transparent surface) highlights the hydrophobicity (neutral = gray dots). The novel inverse agonist **9** (stick model with magenta backbone) is shown compared against the negative image. (E) log P values, ranging from 0.5 to 7.5 (listed 15.11.2017 in the ChEMBL[32]) indicate that lipophilicity is required for potency (pIC$_{50}$ of 3.8–8.9; blue dots). The new inverse agonists follow the same logic (red dots; Table S1). 3QQ (log P = 2.3; pIC$_{50}$ = 6.7), and compound **9** discovered in this study (log P = 3.9; pIC$_{50}$ = 6.2) are circled with green and magenta, respectively.

candidates. The compounds are either designed de novo or screened virtually using computer-aided drug discovery methods before the in vitro testing. Molecular docking mimics flexibly the molecular recognition process between the ligand and its receptor. Despite its widespread use, docking and its rescoring and postprocessing methodologies have case-specific success rates.[27−29] With some targets, the predicted activities correlate well with the experimental data,[30] whereas with others they clearly do not.[31] Agonists, a novel virtual screening (VS) or docking methodology called negative image-based (NIB) screening,[33] were applied here in addition to the standard docking routine.[34,35]

To Improve the Chances of Discovering Novel RORγt Inverse. In NIB screening, a negative image (Figure 1D) is built of the target protein's ligand-binding cavity (Figure 1B) using a specific cavity detection algorithm PANTHER.[33] Next, a set of ligand 3D conformers are generated and compared directly against the cavity-based NIB model using a similarity algorithm ShaEP.[36] On the basis of the shape/electrostatic complementarity of the NIB model and the ligand 3D conformers, the best similarity matches are ranked the highest. This methodology has been shown to function with a wide variety of target proteins such as nuclear receptors and 17β-hydroxysteroid dehydrogenase 1 where ligand-binding cavities are lipophilic.[30,37] Recently, the NIB methodology was shown to improve docking performance by rescoring explicit docking solutions.[38] Furthermore, PANTHER has been used to analyze different ligand-binding cavities for drug discovery purposes.[39,40]

The goal of the study was to discover new RORγt ligands using two different VS techniques that would complement each other in the process. Interestingly, both standard docking and NIB screening put forward mostly the same compounds for experimental testing. Compound selection did not rely solely on the scoring or energy assessment of the software, but docking poses were also inspected critically before their purchase. Altogether, 34 VS hits were purchased and 11 of them were determined to be RORγt inverse agonists with pIC$_{50}$ values ranging from 4.9 (11 μM) to 6.2 (590 nM). Accordingly, testing produced an effective hit rate of 32%—a result that

proves that both of the employed VS methodologies were effective and on an equal footing. Moreover, the discovered compounds represent altogether four structural cores capable of evoking RORγt inverse agonism.

This study expands tangibly the assortment of inverse agonists for RORγt by utilizing two different VS or docking methodologies and human reporter cell-based assay. Understanding the flexibility and druggability of the receptor's active site is vital for unlocking the therapeutic potential of RORγt in autoimmune and inflammatory diseases such as psoriasis or rheumatoid arthritis.

■ RESULTS AND DISCUSSION

Employing Two VS Approaches. Structure-based VS was performed against commercial compound library specs containing >100 000 molecules to discover novel RORγt ligands for experimental testing. VS was performed using two methodologies: (1) molecular docking with GLIDE standard precision(SP)[41] in Maestro and (2) NIB screening with PANTHER/ShaEP-based protocol.[33] Prior to executing VS, both methods were validated with experimental RORγt data (199 active ligands; obtained 1st of June 2015) included in the ChEMBL database.[32] On the basis of the benchmarking with the known active compounds, the early enrichment was excellent for GLIDE SP (Figure S1A) and weaker for NIB screening (Figure S1B). Notably, NIB screening was able to pick all active compounds with pIC$_{50}$ > 7.5 before 10% of the decoys had been screened—a crucial task in which GLIDE slightly failed. The hit candidates discovered using the VS assays were acquired from the specs and analyzed in vitro.

Molecular Docking: Scoring Validation and VS. Docking of the known active ligands with GLIDE SP did not produce high correlation coefficient against the prior experimental data (R^2 = 0.23). On the one hand, the lack of correlation could be explained by the heterogeneous nature of the dataset originating from several laboratories. On the other hand, the success rates and accuracy of the docking algorithms themselves are case-specific and vary accordingly.[27−29] However, a large portion of ligands with pIC$_{50}$ > 7.5 could be effectively separated from those with lower activity by
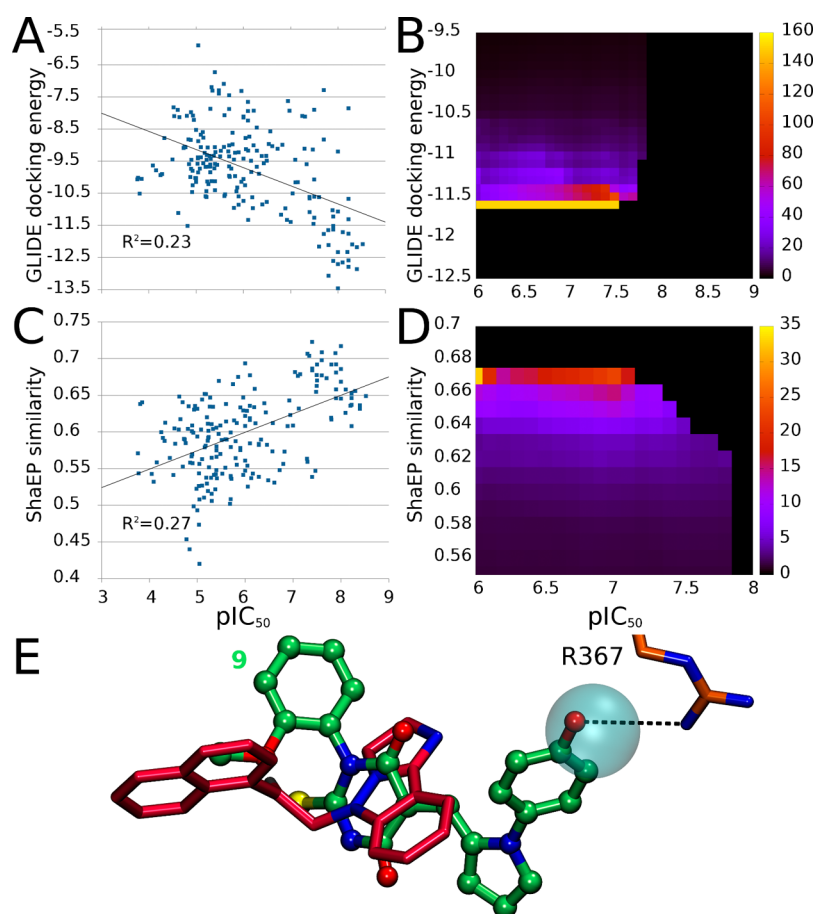
Figure 2. Scoring validation and pharmacophore filtering. (A) In vitro data (x-axis = pIC_{50}) compared to the docking energy (kcal/mol; y-axis) with 199 actives from ChEMBL. (B) Heat map shows that GLIDE docking recognizes potent ligands as their energies fall between −11.6 and −11.4 (N = 20). (C) In vitro data (x-axis: pIC_{50}) set against the ShaEP similarity score (y-axis). Most of the actives are separated (similarity ≥0.67) from the rest of the compounds by NIB screening. (D) When at least 10% of actives were found (N ≥ 20), the heat map shows that the highly active molecules would be discovered with the similarity score of 0.67 using NIB. (E) Several potent inverse agonists H-bond with Arg367 at the sulfate pocket (3QQ in Figure 1A−C) and, thus, a pharmacophore point was used to filter out compounds (stick model with red backbone) unable to make the interaction from NIB screening results. **9** (ball-and-stick model with green backbone) is forming the H-bond based on NIB screening.

GLIDE scoring (Figure 2A). For example, if the docking energy value of −11.6 kcal/mol was used as a cutoff, more than 10% of ligands (N = 20) out of 33 highly active ligands (pIC_{50} > 7.5) could be identified (61%), thus skipping the less active compounds.

The best enrichment (eq 1) for the separation between the potent ligands (pIC_{50} ≥ x but always >6.0) and less active ligands (pIC_{50} < x) is shown in the heat plot (Figure 2B: if only active ones were obtained, value is set to 150). The plot indicates that the GLIDE energy of −11.6 kcal/mol was the most efficient result but also −11.4 and −11.5 kcal/mol could generate >80 enrichment. In general, when the energy was ≤−10.5 kcal/mol, the enrichment remained high. Hence, a cutoff value of −11.4 kcal/mol was used with docking.

Docking of 121 294 molecules, including tautomers and protonation states, yielded 46 molecules with docking energy <−11.4 kcal/mol; from these 24 formed at least one H-bond with the RORγt (G in Table S1). Table S1 shows the log P values, docking scoring values, pIC_{50} values, and the methodology upon which compound selection was based.

Negative Image-Based Screening: Scoring Validation and VS. Because the correlation coefficient for GLIDE docking was weak with the known RORγt ligands, NIB screening was also employed to the task. This alternative docking approach

produced a modest coefficient (R^2 = 0.27; Figure 2C) that was marginally higher than the one provided by GLIDE (R^2 = 0.23). Again, the most potent ligands formed a cluster that could guide the selection process. Note that the enrichment produced by NIB (Figures 2D and S1B) was weaker than that of GLIDE (Figures 2B and S1A). In practice, this suggests that NIB screening is more likely to promote testing of false positives than GLIDE docking. On the basis of the heat plot (Figure 2D), the reasonable cutoff similarity value with NIB would be 0.67, but to remain on the safe side, 0.60 was used instead.

NIB screening of 121 294 molecules yielded 1302 molecules with a similarity value ≥0.67 and 5424 molecules with a value ≥ 0.60. A pharmacophore point (Figure 2E) was used to filter the initial NIB screening results—a process that decreased the number of compounds to 123. The pharmacophore expects polar interaction between the compound (oxygen, nitrogen, fluorine, and chlorine) and the side chain of Arg367 at the sulfate pocket (e.g. 3QQ in Figure 1C). This interaction is expected to improve the binding affinity, but it is not a prerequisite for RORγt binding. When those molecules with unrealistic van der Waals overlap with the protein's main-chain atoms were also removed, **34** compounds remained. Importantly, 22 of them were the same as the ones put
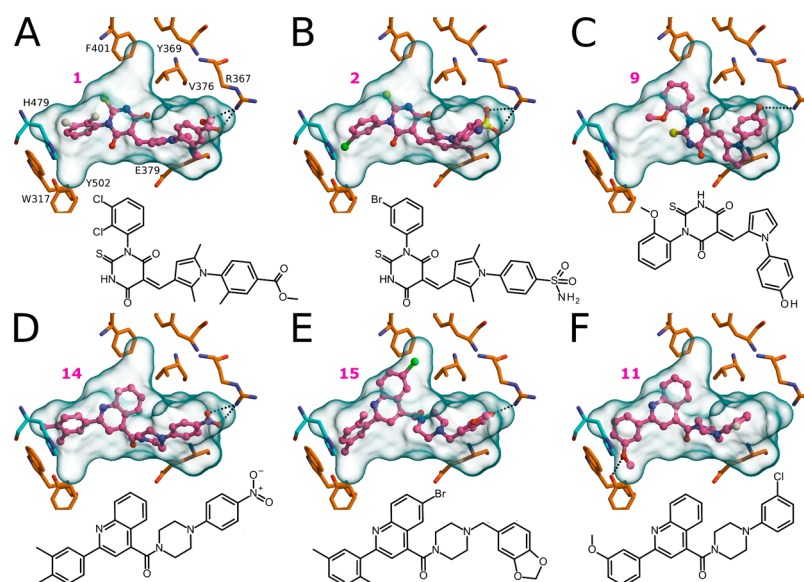
Figure 3. RORγt binding modes of inverse agonists from subsets I and II. The binding suggested by NIB screening for the subset I compounds (A) **1**, (B) **2**, and (C) **9** and subset II compounds (D) **14**, (E) **15**, and (F) **11**. The key residues are shown as sticks (orange backbone), and the cavity's negative image is shown as a transparent surface. The ligands are expected to occupy space next to His479 (cyan backbone) because it controls agonism vs inverse agonism. The H-bonds are shown as dotted lines between polar atoms. The two-dimensional (2D) representations are shown below. The binding modes of **12** and **13**, included in subset II (Table S1; Figure S2), are shown in Figure S3.

forward by GLIDE docking (GP in Table S1). Furthermore, 10 additional molecules were selected for testing (P or (G)P in Table S1), from which three had GLIDE docking energy below −10.5 kcal/mol ((G)P in Table S1).

The VS hit compounds are divided into four subsets (subsets I−IV in Table S1). This division is explained more thoroughly with the predicted ligand-binding modes (see below).

VS Yields Effective Hit Rate of 32%. The IC_{50} value of the most potent compound **9** (pIC$_{50}$ = 6.2; Table S1) was determined to be in the nanomolar range (587 nM; Table S1) based on the experimental testing. Most of the remaining compounds fell into the micromolar range with values between the first and the second concentration on the dilution series (Table S1). The less active molecules were given values outside the dilution series, and thus, these numbers should be considered as approximate results only. The IC_{50} value of ursolic acid was determined to be 112 nM based on the average of two control measurements. For comparison, this result for the control is well in line with the previously measured IC_{50} values.[42] The somewhat lackluster potency is stereotypical for pure VS-based drug discovery projects, in which the most promising hit compounds are not refined further under the systematic organic synthesis programme. Nevertheless, the effective hit rate of the screening was 32%—a clear indication that the applied VS assays were able to pick RORγt inverse agonists from the vast compound library with confidence.

Four Cores Producing Inverse Agonism. The tested 34 molecules were divided into subsets I−IV (Table S1) based on their structural cores for detailed structure−activity relationship (SAR) analysis (Figures 3, S2 and S4). Both VS methods produced similar binding poses for the compounds, and accordingly, the SAR analysis focuses only on the poses outputted by NIB screening. Pan assay interference (PAINS) filtering indicates that compounds **1**−**10** as well as **14**, **16**, **31**, and **34** belong potentially to the PAINS category, which could reduce their applicability as drugs.

Subset I. The second largest set of molecules (**1**−**10** in Table S1) contains a thiobarbituric acid-moiety, making them reactive and, consequently, not optimal for pharmaceutical purposes. Compounds **1**, **2**, and **9** were found active (Figure 3A−C; Table S1). Although both **1** and **2** extend from the vicinity of Arg367 to the area next to His479 and Tyr502 inside the cavity (Figure 3A,B), only **9** produces a tight fit with the cavity facing Arg367 (Figure 3C). However, **9** does not extend into all of the subcavities (Figure 3C). The rest of the compounds (**3**−**8** and **10** in Table S1) were found inactive. Supporting Information Figures S2 and S3 contain, respectively, the 2D representations and predicted binding poses for all of the inactive compounds.

Subset II. A set of seven [4-(phenyl)piperazin-1-yl]-(2-phenyl-4-quinolyl)methanone derivatives were tested for RORγt activity (**11**−**17** in Table S1; Figures 3D−F and S2). Compounds **16** and **17** were either insoluble or inactive (Table S1; Figures S2 and S3). The activities of **14**, **15**, and **11** (Figure 3D−F) are roughly at the same level (IC_{50}: 2.0−2.2 μM; Table S1). Tyr502 forms an H-bond with the methoxy of **11** (Figure 3F); meanwhile, **14** and **15** H-bond with Arg367 (Figure 3D,E), although the angles are less than optimal. The bromine of **15** improves the binding by filling the hydrophobic cavity end formed by Tyr369, Val376, and Phe401 (Figure 3E). The two less active molecules **12** and **13** (Table S1; Figures S2 and S3) have a CF_3 group that aligns favorably next to the side chain of Arg367 (Figure S3); however, both of them align poorly next to Tyr502 (Figure S3). For example, **13** protrudes a hydrophobic methyl group into a subcavity that would be optimal for an H-bond acceptor (Figure S3). The inactivity of **17** results from the fact that its fluorine moiety cannot extend near Arg367; furthermore, its methyl group cannot fit next to Tyr502 (Figures S2 and S3). In short, the subset II core is an excellent fit for the cavity, but none of the compounds had all three groups—nitro, bromine, and methoxy—at the optimal positions.

Subset III. Compounds **18**−**21** (Figures S2 and S4A,B), housing a four-ring system, were selected for testing by both in

silico assays (Table S1). The hydrophobic system is a good fit with the cavity controlling the agonism versus inverse agonism function of RORγt (Figures S3 and S4A,B). Furthermore, both **18** and **19** accept a hydrogen from the main chain nitrogen of Glu379 (Figure S4A,B), which ensures activity (Table S1). In contrast, **20** and **21** cannot secure the same H-bond using their nitro- and acid-groups without compromising the favorable binding interactions elsewhere in the cavity (Figure S3). This renders **20** and **21** inactive in testing (Table S1).

Subset IV. Compound **34** (Figure S4C) was not a preferred choice for the activity testing based on scoring (Table S1; Figure S6), although it could not extend to the vicinity of His479 and Tyr502 in the cavity (Figure S4C). Nevertheless, **34** was selected because of its ability to H-bond with and fill the cavity near Arg367. The placement of the two bromines was predicted to be enough to force the protein into the inverse agonist conformation (Figure S4C). Although the in vitro testing verified this hypothesis (Table S1), **34** is not a particularly potent inverse agonist (pIC$_{50}$ = 5.0 μM). The other compounds included in this largest subset (**23−33** in Table S1; Figures S2 and S5) were inactive.

■ CONCLUSIONS

VS identified 11 hits out of 34 experimentally tested compounds, thus yielding a hit rate of 32% (Table S1). Nine hits were identified by both standard molecular docking and NIB screening. Moreover, two compounds were discovered using only NIB screening. NIB screening results were refined using pharmacophore filtering (Figure 2E). The fact that both VS methodologies could discover mostly the same inverse agonists is encouraging because NIB screening is considerably faster than standard molecular docking algorithms. Accordingly, NIB screening is a suitable method for screening RORγt inverse agonists especially when considering its computational costs. The most potent hit (**9** in Table S1 and Figure 3C) was nearly correctly scored and predicted by both the VS assays. However, the binding favorability of the other hits was clearly overestimated by both the methods (Table S1). As a result of this study, the diversity of novel RORγt inverse agonists is expanded substantially because of the discovery of four new structural cores.

■ MATERIALS AND METHODS

Ligand Preparation. The Simplified Molecular-Input Line-Entry System (SMILES) strings of ligands (Supporting Information) were converted to 3D structures, including possible tautomers and protonation states, with LigPrep in Maestro 2015-1 (Schrödinger, LLC, New York, NY, USA, 2017) with an enhanced planarity option at pH 7.4 ± 0.0 by using Merck molecular force field 94 (MMFF94).[43] For rigid docking purposes, multiple low-energy conformations were generated with ConfGen.[44]

Compounds for Screening Method Validation. Validated ligands for RORγt were retrieved from the ChEMBL[32] from 502 IC$_{50}$ results for human RORγt (obtained 9th of June 2015), 199 had been reported active, and thus these compounds were used to validate the VS assays. When several activity measurements were available for the same compound, the one suggested as best was used. The activity data were converted into pIC$_{50}$ (−log(IC$_{50}$)).

Compounds for VS. A commercially available compound collection specs (Specs, The Netherlands; www.specs.net; 10

mg compound library 05/2014) was used. Modified drug-like options were used, where the molecular weight was set to 250 < MW < 600 and the number of rotatable bonds was set to a maximum of 6. The latter option was set to speed up the VS and to enhance the probability that the identified ligands would be selective for the target. Furthermore, because the existing high-affinity RORγt ligands are highly lipophilic (Figure 1B), only molecules with log $P \geq 7.0$ were removed. In total, the used VS library consists of 116 495 molecules or 121 294 when including tautomers and different protonation states.

Protein Structure Preparation. At the time of performing the VS assays (5/2015), there were 12 structures available for RORγt at the Protein Data Bank.[45] Because our aim was to identify (agonist/inverse agonist) ligands for RORγt, a high-resolution structure (1.7 Å) for RORγt with bound partial inverse agonist was selected (PDB; 4WLB[46]). All of the available structures were tested initially for the VS use (data not shown); however, 4WLB was found to produce the best results in the benchmarking. The same protein structure was used both in PANTHER/ShaEP-based NIB screening[33] and GLIDE-based docking.[41] In both cases, the protein preparation Wizard included in Maestro 2015-1 (Schrödinger, LLC, New York, NY, USA, 2017) was employed with the following options: (1) import and process: delete waters, preprocess; (2) review and modify: delete chain B, C, E, delete A: TLA602, TLA603 (tartaric acids); and (3) refine: use PROPKA pH: 7.4, optimize.

Molecular Docking. Molecular docking of the small molecules was performed using GLIDE in Maestro with SP. The centroid coordinates of the partial inverse agonist bound in the target protein structure (3QQ in Figure 1A−C; PDB: 4WLB) were used as the binding site center in the docking. A radius of 10 Å was used in grid generation. As stated above, a number of alternative ligand conformers were generated to improve the docking sampling.

Negative Image-Based Screening. The NIB model consisting of optimally positioned polar and neutral cavity filling atoms (Figure 1D) was produced using PANTHER.[33] The NIB model was compared against multiple low-energy ligand 3D conformations (compound **9** vs NIB model in Figure 1D) using similarity comparison algorithm ShaEP.[36] While GLIDE typically rejects molecules that overlap with the protein, ShaEP imposes only a marginal penalty for such overlaps during the similarity comparison. Accordingly, both docking methods should identify compounds that fit perfectly (a very rare occurrence) but behave in a markedly different way if the space available for the binding is exceeded. Mainly, the NIB screening provides more flexibility to ligand−receptor complex formation, and GLIDE-based docking is more likely to discard compounds because of minor coordinate overlaps with the protein.

VS Efficiency. To estimate the validity of the generated NIB models and molecular docking settings, several strategies were employed. First, the correlation coefficients were used for docking scoring values against experimental pIC$_{50}$ values. Second, the pIC$_{50}$ and GLIDE docking energy (kcal/mol) or ShaEP similarity values in Figure 2 were used to generate representative heat plots using gnuplot-5.0 (www.gnuplot.info). Heat plots were used to visualize the efficiency of the used method to separate those active ligands that have a pIC$_{50}$ value above the given value from those below the same value, for example, how well the known ligands with pIC$_{50}$ above 7.0 are recognized over those with pIC$_{50}$ below 7.0. For heat maps, the enrichment (eq 1) was calculated with the increment of 0.1

from pIC_{50} 6.0, until the number of the active ligands in the given threshold value was below 10.0.

$$\text{Enrichment} = \frac{\text{NaG}/\text{Na}}{\text{NiG}/\text{Ni}} \quad (1)$$

where NaG = number of ligands with $\leq$ GLIDE docking energy and above pIC_{50}, Na = total number of ligands above pIC_{50}, NiG = number of ligands with $\leq$ GLIDE docking energy and below pIC_{50}, and Ni = total number of ligands below pIC_{50}.

Pharmacophore Filtering. To improve the NIB screening yield, a carefully selected 1 Å-radius pharmacophore filter point was used (Figure 2E). Only those docked molecules that formed polar interactions with the receptor and did not have hydrophobic groups in the proximity to the NH1 atom of the Arg367 side chain were selected. The guanidinium group acts as a H-bond donor for many RORγt high-affinity ligands (e.g. 3QQ in Figure 1C) and, accordingly, it was chosen for postprocessing or filtering using the soon-to-be-published in-house algorithm SDFCONF (Lätti et al. manuscript in preparation).

PAINS Filtering. PAINS compounds filtering was performed by the PAINS3 filter (or A filter) in Canvas module in Maestro 9. The filtering suggests that compounds **1−10** (= subset I) as well as **14**, **16**, **31**, and **34** belong potentially to the PAINS category. This suggests that roughly half of the compounds could be promiscuous and require further experimental testing and/or modification before they could be used as RORγt inverse agonists or as drug candidates for any other target.

Experimental Testing. The activity of the 34 selected molecules (Table S1) was determined at 5 μM concentration using the Human RAR-related Orphan Receptor Gamma Reporter Assay System in a 96-well format (Indigo Biosciences, PA, USA). The assay utilizes human reporter cells designed to express high levels of human RORγ hybrids of both isoforms 1 and 2, capable of quantifying inverse agonism and agonism. The assay was performed as a two data point analysis, and 11 molecules exhibiting the strongest activity were selected for further analysis. The same kit was used to determine the IC_{50} values for the most promising molecules. The dilution series protocol of the kit for the final concentrations was followed. The concentrations of the tested molecules ranged from 6 μM to 8 nM in 1/3-fold decrements, and each concentration was measured three times. In addition, the maximum signal was determined as 0 nM concentration, and the minimum signal was measured from the wells lacking cells. Luminescence was measured with VICTOR X4 Multilabel Plate Reader (PerkinElmer, MA, USA) using luminometry technology. Before reading the plate, 5 s plate shake was performed as instructed and each well was then read after >5 min incubation for 0.5 s based on counts/s label.

The results were normalized using GraphPad Prism 5.03 (GraphPad Software, Inc., CA, USA). On the basis of the results, the maximal signal of 0 nM concentration was determined to be reached at 10^{-9} M because of the fact that all of the measured molecules reached approximately the maximal signal already at the previous dilution. The minimum signal was reached either at 10^{-4} or 10^{-3} M concentration depending on the behavior of the molecule on the dilution series. The goal was rather to underestimate than overestimate the potency of each molecule. The normalized results were fitted on a curve with nonlinear regression using the equation for −log[inhibitor] versus response in GraphPad Prism (Figure

S6), and the IC_{50} values were determined/approximated based on this curve fit (Table S1). Because most of the active compounds found in this study were in the proximity of the maximal tested concentration, the sigmoidal curve fit is not optimal. As described in the analysis kit, ursolic acid was used as a control molecule for the experiment, and its IC_{50} value was determined twice during the course of the experiment. Because the curve fit of ursolic acid reached the top and bottom plateaus already on the dilution series, there was no need to approximate the top and bottom concentrations and those were left out when analyzing ursolic acid.

Figure Preparation. Figures 1A−D and 2E were prepared using BODIL[47] and VMD 1.9.2.[48] Figures 3A−D and S3−S5 were prepared using BODIL, MolScript2.1.2204[49] and Raster3D 3.0.2.[50] BIOVIA Draw 16.1 (San Diego: Dassault Systèmes, 2017) was used to generate 2D representations in Figures 3, S2, and S4. The area under curve (AUC) values and the early enrichment values were calculated with Rocker0.1.4.[51] The enrichment factors were calculated as true positive rates when 1% of the decoy molecules (here the entire specs compound set) have been found. The standard deviation for the AUC is acquired with the derived error for the Wilcoxon statistic.[52]

■ ASSOCIATED CONTENT

Ⓢ Supporting Information

The Supporting Information is available free of charge on the ACS Publications website at DOI: 10.1021/acsomega.8b00603.

> Computational and experimental results with the screened compounds, 2D representations of subsets I−IV compounds, predicted poses of subsets I−III compounds, RORγt binding modes of inverse agonists of from subsets III and IV, predicted poses for the subset IV compounds, and IC50 plots for γt agonists (PDF)
> Retrieved SMILES codes for ligands (TXT)

■ AUTHOR INFORMATION

Corresponding Author

*E-mail: olli.pentikainen@utu.fi (O.T.P.).

ORCID Ⓘ

Sanna Rauhamäki: 0000-0002-3014-3120
Pekka A. Postila: 0000-0002-2947-7991
Klaus R. Liedl: 0000-0002-0985-2299
Olli T. Pentikäinen: 0000-0001-7188-4016

Author Contributions

O.T.P. and K.R.L. designed the study. O.T.P., S.N., and E.M. performed VS. S.R. performed the in vitro assay. S.R., P.A.P., and O.T.P. performed the analysis. S.L. did the pharmacophore filtering. O.T.P., S.R., P.A.P., S.L., and K.R.L. wrote the manuscript. All authors have given approval to the final version of the manuscript.

Notes

The authors declare no competing financial interest.

■ ACKNOWLEDGMENTS

■ ABBREVIATIONS

RORγt, retinoic acid-related orphan receptor γt; TH17, T-helper 17 cells; NIB, negative image-based; SAR, structure−activity relationship; H-bond, hydrogen bond

■ REFERENCES

(1) He, Y.-W.; Deftos, M. L.; Ojala, E. W.; Bevan, M. J. RORγt, a Novel Isoform of an Orphan Receptor, Negatively Regulates Fas Ligand Expression and IL-2 Production in T Cells. *Immunity* **1998**, *9*, 797−806.

(2) Ivanov, I. I.; McKenzie, B. S.; Zhou, L.; Tadokoro, C. E.; Lepelley, A.; Lafaille, J. J.; Cua, D. J.; Littman, D. R. The Orphan Nuclear Receptor RORγt Directs the Differentiation Program of Proinflammatory IL-17+ T Helper Cells. *Cell* **2006**, *126*, 1121−1133.

(3) Littman, D. R.; Rudensky, A. Y. Th17 and Regulatory T Cells in Mediating and Restraining Inflammation. *Cell* **2010**, *140*, 845−858.

(4) Bronner, S. M.; Zbieg, J. R.; Crawford, J. J. RORγ Antagonists and Inverse Agonists: A Patent Review. *Expert Opin. Ther. Pat.* **2017**, *27*, 101−112.

(5) Smith, S. H.; Peredo, C. E.; Takeda, Y.; Bui, T.; Neil, J.; Rickard, D.; Millerman, E.; Therrien, J.-P.; Nicodeme, E.; Brusq, J.-M.; Birault, V.; Viviani, F.; Hofland, H.; Jetten, A. M.; Cote-Sierra, J. Development of a Topical Treatment for Psoriasis Targeting RORγ: From Bench to Skin. *PLoS One* **2016**, *11*, No. e0147979.

(6) Wang, J.; Zou, J. X.; Xue, X.; Cai, D.; Zhang, Y.; Duan, Z.; Xiang, Q.; Yang, J. C.; Louie, M. C.; Borowsky, A. D.; Gao, A. C.; Evans, C. P.; Lam, K. S.; Xu, J.; Kung, H.-J.; Evans, R. M.; Xu, Y.; Chen, H.-W. ROR-γ Drives Androgen Receptor Expression and Represents a Therapeutic Target in Castration-Resistant Prostate Cancer. *Nat. Med.* **2016**, *22*, 488−496.

(7) Fauber, B. P.; Magnuson, S. Modulators of the Nuclear Receptor Retinoic Acid Receptor-Related Orphan Receptor-γ (RORγ or RORc). *J. Med. Chem.* **2014**, *57*, 5871−5892.

(8) René, O.; Fauber, B. P.; Boenig, G. d. L.; Burton, B.; Eidenschenk, C.; Everett, C.; Gobbi, A.; Hymowitz, S. G.; Johnson, A. R.; Kiefer, J. R.; Liimatta, M.; Lockey, P.; Norman, M.; Ouyang, W.; Wallweber, H. A.; Wong, H. Minor Structural Change to Tertiary Sulfonamide RORC Ligands Led to Opposite Mechanisms of Action. *ACS Med. Chem. Lett.* **2015**, *6*, 276−281.

(9) Khan, P. M.; El-Gendy, B. E. D. M.; Kumar, N.; Garcia-Ordonez, R.; Lin, L.; Ruiz, C. H.; Cameron, M. D.; Griffin, P. R.; Kamenecka, T. M. Small Molecule Amides as Potent ROR-γ Selective Modulators. *Bioorg. Med. Chem. Lett* **2013**, *23*, 532−536.

(10) Kumar, N.; Solt, L. A.; Conkright, J. J.; Wang, Y.; Istrate, M. A.; Busby, S. A.; Garcia-ordonez, R. D.; Burris, T. P.; Griffin, P. R. The Benzenesulfoamide T0901317 [N- (2, 2, 2-Trifluoroethyl) -N-Benzenesulfonamide] Is a Novel Retinoic Acid Receptor- Related Orphan Receptor-α/γ Inverse Agonist. *Mol. Pharmacol.* **2010**, *77*, 228−236.

(11) Nishiyama, Y.; Nakamura, M.; Misawa, T.; Nakagomi, M.; Makishima, M.; Ishikawa, M.; Hashimoto, Y. Structure-Activity Relationship-Guided Development of Retinoic Acid Receptor-Related Orphan Receptor Gamma (RORγ)-Selective Inverse Agonists with a Phenanthridin-6(5H)-One Skeleton from a Liver X Receptor Ligand. *Bioorg. Med. Chem.* **2014**, *22*, 2799−2808.

(12) Solt, L. A.; Banerjee, S.; Campbell, S.; Kamenecka, T. M.; Burris, T. P. ROR Inverse Agonist Suppresses Insulitis and Prevents Hyperglycemia in a Mouse Model of Type 1 Diabetes. *Endocrinology* **2015**, *156*, 869−881.

(13) Kumar, N.; Lyda, B.; Chang, M. R.; Lauer, J. L.; Solt, L. A.; Burris, T. P.; Kamenecka, T. M.; Griffin, P. R. Identification of SR2211: A Potent Synthetic RORγ-Selective Modulator. *ACS Chem. Biol.* **2012**, *7*, 672−677.

(14) Solt, L. A.; Kumar, N.; He, Y.; Kamenecka, T. M.; Griffin, P. R.; Burris, T. P. Identification of a Selective RORγ Ligand That Suppresses T H17 Cells and Stimulates T Regulatory Cells. *ACS Chem. Biol.* **2012**, *7*, 1515−1519.

(15) Solt, L. A.; Kumar, N.; Nuhant, P.; Wang, Y.; Lauer, J. L.; Liu, J.; Istrate, M. A.; Kamenecka, T. M.; Roush, W. R.; Vidović, D.; Schürer, S. C.; Xu, J.; Wagoner, G.; Drew, P. D.; Griffin, P. R.; Burris, T. P. Suppression of TH17 Differentiation and Autoimmunity by a Synthetic ROR Ligand. *Nature* **2011**, *472*, 491−494.

(16) Gege, C.; Schlüter, T.; Hoffmann, T. Identification of the First Inverse Agonist of Retinoid-Related Orphan Receptor (ROR) with Dual Selectivity for RORβ and RORγt. *Bioorg. Med. Chem. Lett* **2014**, *24*, 5265−5267.

(17) Toyama, H.; Nakamura, M.; Hashimoto, Y.; Fujii, S. Design and Synthesis of Novel ROR Inverse Agonists with a Dibenzosilole Scaffold as a Hydrophobic Core Structure. *Bioorg. Med. Chem.* **2015**, *23*, 2982−2988.

(18) Huh, J. R.; Englund, E. E.; Wang, H.; Huang, R.; Huang, P.; Rastinejad, F.; Inglese, J.; Austin, C. P.; Johnson, R. L.; Huang, W.; Littman, D. R. Identification of Potent and Selective Diphenylpropa-namide RORγ Inhibitors. *ACS Med. Chem. Lett.* **2013**, *4*, 79−84.

(19) Kumar, N.; Kamenecka, T.; Lyda, B.; Khan, P.; Chang, M. R.; Garcia-Ordonez, R. D.; Cameron, M.; Ferguson, J.; Mercer, B. A.; Hodder, P.; Rosen, H.; Griffin, P. R. Identification of a Novel Selective Inverse Agonist Probe and Analogs for the Retinoic Acid Receptor-Related Orphan Receptor Gamma (RORγ) 2012 Apr 16 [Updated 2013 Mar 14]. Probe Reports from NIH Mol. Libr. Progr. [Internet]. Bethesda Natl. Cent. Biotechnol. Inf.

(20) Jin, L.; Martynowski, D.; Zheng, S.; Wada, T.; Xie, W.; Li, Y. Structural Basis for Hydroxycholesterols as Natural Ligands of Orphan Nuclear Receptor RORγ. *Mol. Endocrinol.* **2010**, *24*, 923−929.

(21) Olsson, R. I.; Xue, Y.; von Berg, S.; Aagaard, A.; McPheat, J.; Hansson, E. L.; Bernström, J.; Hansson, P.; Jirholt, J.; Grindebacke, H.; Leffler, A.; Chen, R.; Xiong, Y.; Ge, H.; Hansson, T. G.; Narjes, F. Benzoxazepines Achieve Potent Suppression of IL-17 Release in Human T-Helper 17 (T H 17) Cells through an Induced-Fit Binding Mode to the Nuclear Receptor RORγ. *ChemMedChem* **2016**, *11*, 207−216.

(22) Fauber, B. P.; René, O.; de Leon Boenig, G.; Burton, B.; Deng, Y.; Eidenschenk, C.; Everett, C.; Gobbi, A.; Hymowitz, S. G.; Johnson, A. R.; La, H.; Liimatta, M.; Lockey, P.; Norman, M.; Ouyang, W.; Wang, W.; Wong, H. Reduction in Lipophilicity Improved the Solubility, Plasma-Protein Binding, and Permeability of Tertiary Sulfonamide RORc Inverse Agonists. *Bioorg. Med. Chem. Lett* **2014**, *24*, 3891−3897.

(23) Hintermann, S.; Guntermann, C.; Mattes, H.; Carcache, D. A.; Wagner, J.; Vulpetti, A.; Billich, A.; Dawson, J.; Kaupmann, K.; Kallen, J.; Stringer, R.; Orain, D. Synthesis and Biological Evaluation of New Triazolo- and Imidazolopyridine RORγt Inverse Agonists. *ChemMedChem* **2016**, *11*, 2640−2648.

(24) Postila, P. A.; Swanson, G. T.; Pentikäinen, O. T. Exploring Kainate Receptor Pharmacology Using Molecular Dynamics Simulations. *Neuropharmacology* **2010**, *58*, 515−527.

(25) Leanne Lash-Van Wyhe, L.; Postila, P. A.; Tsubone, K.; Sasaki, M.; Pentikäinen, O. T.; Sakai, R.; Swanson, G. T. Pharmacological Activity of C10-Substituted Analogs of the High-Affinity Kainate Receptor Agonist Dysiherbaine. *Neuropharmacology* **2010**, *58*, 640−649.

(26) Postila, P. A.; Ylilauri, M.; Pentikäinen, O. T. Full and Partial Agonism of Ionotropic Glutamate Receptors Indicated by Molecular Dynamics Simulations. *J. Chem. Inf. Model.* **2011**, *51*, 1037−1047.

(27) McGaughey, G. B.; Sheridan, R. P.; Bayly, C. I.; Culberson, J. C.; Kreatsoulas, C.; Lindsley, S.; Maiorov, V.; Truchon, J.-F.; Cornell, W. D. Comparison of Topological, Shape, and Docking Methods in Virtual Screening. *J. Chem. Inf. Model.* **2007**, *47*, 1504−1519.

(28) Mohan, V.; Gibbs, A.; Cummings, M.; Jaeger, E.; DesJarlais, R. Docking: Successes and Challenges. *Curr. Pharm. Des.* **2005**, *11*, 323−333.

(29) Virtanen, S. I.; Niinivehmas, S. P.; Pentikäinen, O. T. Case-Specific Performance of MM-PBSA, MM-GBSA, and SIE in Virtual Screening. *J. Mol. Graph. Model.* **2015**, *62*, 303−318.

(30) Niinivehmas, S. P.; Manivannan, E.; Rauhamäki, S.; Huuskonen, J.; Pentikäinen, O. T. Identification of Estrogen Receptor α Ligands

with Virtual Screening Techniques. *J. Mol. Graph. Model.* **2016**, *64*, 30−39.

(31) Shubina, V.; Niinivehmas, S.; Pentikainen, O. Reliability of Virtual Screening Methods in Prediction of PDE4Binhibitor Activity. *Curr. Drug Discovery Technol.* **2015**, *12*, 117−126.

(32) Gaulton, A.; Bellis, L. J.; Bento, A. P.; Chambers, J.; Davies, M.; Hersey, A.; Light, Y.; McGlinchey, S.; Michalovich, D.; Al-Lazikani, B.; Overington, J. P. ChEMBL: A Large-Scale Bioactivity Database for Drug Discovery. *Nucleic Acids Res.* **2012**, *40*, D1100−D1107.

(33) Niinivehmas, S. P.; Salokas, K.; Lätti, S.; Raunio, H.; Pentikäinen, O. T. Ultrafast Protein Structure-Based Virtual Screening with Panther. *J. Comput. Aided Mol. Des.* **2015**, *29*, 989−1006.

(34) Niinivehmas, S. P.; Virtanen, S. I.; Lehtonen, J. V.; Postila, P. A.; Pentikäinen, O. T. Comparison of Virtual High-Throughput Screening Methods for the Identification of Phosphodiesterase-5 Inhibitors. *J. Chem. Inf. Model.* **2011**, *51*, 1353−1363.

(35) Virtanen, S. I.; Pentikäinen, O. T. Efficient Virtual Screening Using Multiple Protein Conformations Described as Negative Images of the Ligand-Binding Site. *J. Chem. Inf. Model.* **2010**, *50*, 1005−1011.

(36) Vainio, M. J.; Puranen, J. S.; Johnson, M. S. ShaEP: Molecular Overlay Based on Shape and Electrostatic Potential. *J. Chem. Inf. Model.* **2009**, *49*, 492−502.

(37) Niinivehmas, S.; Postila, P. A.; Rauhamäki, S.; Manivannan, E.; Kortet, S.; Ahinko, M.; Huuskonen, P.; Nyberg, N.; Koskimies, P.; Lätti, S.; Multamäki, E.; Juvonen, R. O.; Raunio, H.; Pasanen, M.; Huuskonen, J.; Pentikäinen, O. T. Blocking Oestradiol Synthesis Pathways with Potent and Selective Coumarin Derivatives. *J. Enzyme Inhib. Med. Chem.* **2018**, *33*, 743−754.

(38) Kurkinen, S. T.; Niinivehmas, S.; Ahinko, M.; Lätti, S.; Pentikäinen, O. T.; Postila, P. A. Improving Docking Performance Using Negative Image-Based Rescoring. *Front. Pharmacol.* **2018**, *9*, 260.

(39) Rauhamäki, S.; Postila, P. A.; Niinivehmas, S.; Kortet, S.; Schildt, E.; Pasanen, M.; Manivannan, E.; Ahinko, M.; Koskimies, P.; Nyberg, N.; Huuskonen, P.; Multamäki, E.; Pasanen, M.; Juvonen, R. O.; Raunio, H.; Huuskonen, J.; Pentikäinen, O. T. Structure-Activity Relationship Analysis of 3-Phenylcoumarin-Based Monoamine Oxidase B Inhibitors. *Front. Chem.* **2018**, *6*, 41.

(40) Juvonen, R. O.; Rauhamäki, S.; Kortet, S.; Niinivehmas, S.; Troberg, J.; Petsalo, A.; Huuskonen, J.; Raunio, H.; Finel, M.; Pentikäinen, O. T. Molecular Docking-Based Design and Development of a Highly Selective Probe Substrate for UDP-Glucuronosyl-transferase 1A10. *Mol. Pharm.* **2018**, *15*, 923−933.

(41) Friesner, R. A.; Banks, J. L.; Murphy, R. B.; Halgren, T. A.; Klicic, J. J.; Mainz, D. T.; Repasky, M. P.; Knoll, E. H.; Shelley, M.; Perry, J. K.; Shaw, D. E.; Francis, P.; Shenkin, P. S. Glide: A New Approach for Rapid, Accurate Docking and Scoring. 1. Method and Assessment of Docking Accuracy. *J. Med. Chem.* **2004**, *47*, 1739−1749.

(42) Zhang, Y.; Xue, X.; Jin, X.; Song, Y.; Li, J.; Luo, X.; Song, M.; Yan, W.; Song, H.; Xu, Y. Discovery of 2-Oxo-1,2-Dihydrobenzo[cd]-indole-6-Sulfonamide Derivatives as New RORγ Inhibitors Using Virtual Screening, Synthesis and Biological Evaluation. *Eur. J. Med. Chem.* **2014**, *78*, 431−441.

(43) Halgren, T. A. Potential Energy Functions. *Curr. Opin. Struct. Biol.* **1995**, *5*, 205−210.

(44) Watts, K. S.; Dalal, P.; Murphy, R. B.; Sherman, W.; Friesner, R. A.; Shelley, J. C. ConfGen: A Conformational Search Method for Efficient Generation of Bioactive Conformers. *J. Chem. Inf. Model.* **2010**, *50*, 534−546.

(45) Berman, H. M.; Westbrook, J.; Feng, Z.; Gilliland, G.; Bhat, T. N.; Weissig, H.; Shindyalov, I. N.; Bourne, P. E. The Protein Data Bank. *Nucleic Acids Res.* **2000**, *28*, 235−242.

(46) Van Niel, M. B.; Fauber, B. P.; Cartwright, M.; Gaines, S.; Killen, J. C.; René, O.; Ward, S. I.; De Leon Boenig, G.; Deng, Y.; Eidenschenk, C.; Everett, C.; Gancia, E.; Ganguli, A.; Gobbi, A.; Hawkins, J.; Johnson, A. R.; Kiefer, J. R.; La, H.; Lockey, P.; Norman, M.; Ouyang, W.; Qin, A.; Wakes, N.; Waszkowycz, B.; Wong, H. A Reversed Sulfonamide Series of Selective RORc Inverse Agonists. *Bioorg. Med. Chem. Lett* **2014**, *24*, 5769−5776.

(47) Lehtonen, J. V.; Still, D.-J.; Rantanen, V.-v.; Ekholm, J.; Björklund, D.; Iftikhar, Z.; Huhtala, M.; Repo, S.; Jussila, A.; Jaakkola, J.; Pentikäinen, O.; Nyrönen, T.; Salminen, T.; Gyllenberg, M.; Johnson, M. S. BODIL: A Molecular Modeling Environment for Structure-Function Analysis and Drug Design. *J. Comput. Aided Mol. Des.* **2004**, *18*, 401−419.

(48) Humphrey, W.; Dalke, A.; Schulten, K. VMD: Visual Molecular Dynamics. *J. Mol. Graph.* **1996**, *14*, 33−38.

(49) Kraulis, P. J. MOLSCRIPT: A Program to Produce Both Detailed and Schematic Plots of Protein Structures. *J. Appl. Crystallogr.* **1991**, *24*, 946−950.

(50) Merritt, E. A.; Bacon, D. J. Raster3D: Photorealistic Molecular Graphics. *Methods Enzymol.* **1997**, *277*, 505−524.

(51) Lätti, S.; Niinivehmas, S.; Pentikäinen, O. T. Rocker: Open Source, Easy-to-Use Tool for AUC and Enrichment Calculations and ROC Visualization. *J. Cheminf.* **2016**, *8*, 45.

(52) Hanley, A. J.; McNeil, J. B. The Meaning and Use of the Area under a Receiver Operating Characteristic (ROC) Curve. *Radiology* **1982**, *143*, 29−36.